Advancing Proton-Conducting Ceramic Cells with Thin Electrolyte Layers Prepared by Wet Powder Spraying

Yuan Zeng*[1, 2], Moritz Kindelmann[1, 3], Rishad Kunafiev[4], Mariya E. Ivanova[1], Olivier Guillon[1, 2, 5], Kwati Leonard*[4], Norbert H. Menzler[1,2]

1 Forschungszentrum Jülich GmbH, Institute of Energy Materials and Devices IMD-2: Materials Synthesis and Processing, 52425 Jülich, Germany

2 Department of Ceramics and Refractory Materials, Institute of Mineral Engineering, RWTH Aachen University, 52064 Aachen, Germany

3 Forschungszentrum Jülich GmbH, Ernst Ruska Center for Microscopy and Spectroscopy with Electrons (ER-C 2), 52425 Jülich, Germany

4 International Institute for Carbon Neutral Energy Research (WPI-I2CNER), Kyushu University 744 Motooka, Nishiku, Fukuoka 819-0395, Japan

5 Jülich-Aachen Research Alliance: JARA-Energy, 52425 Jülich, Germany

Corresponding author's email: y.zeng@fz-juelich.de; kwati@i2cner.kyushu-u.ac.jp

Abstract:

The development of proton conducting high temperature solid state electrochemical cells (PCCs) is vital for energy conversion and storage. Here, a $SrZr_{0.5}Ce_{0.4}Y_{0.1}O_{3-\delta}$ (SZCY) / NiO supported cell with a 3 μm $BaZr_{0.16}Ce_{0.64}Y_{0.1}Yb_{0.1}O_{3-\delta}$ electrolyte, deposited by wet powder spraying (WPS), was fabricated. Co-sintering at 1375 °C yielded a dense electrolyte layer with large grains. Sr diffusion from the SZCY substrate compensated for Ba evaporation, preventing the formation of Y-rich secondary phases and thereby enhancing sinterability. STEM confirmed elemental diffusion and verified the proton transport without grain boundary obstruct in the thin electrolyte layer. The fabricated PCC achieved 422 mW cm^{-2} at 0.7 V and 600 °C in fuel cell mode, demonstrating competitive electrochemical performance. Minor defects in the electrolyte layer contributed to reduced open-circuit voltage (OCV) at lower temperatures, attributed to contamination during substrate pre-treatment. This work demonstrates the viability of WPS for scalable fabrication of thin PCC electrolyte layers with enhanced electrochemical performance.

Keywords: Proton conducting cells; Wet powder spraying; BZCYYb; Thin electrolyte; Lower sintering temperature

1. Introduction

Amidst global energy challenges, the development of clean energy is key to achieving sustainable development by effectively reducing carbon emissions and optimizing the energy infrastructure. Proton-conducting high temperature solid-state electrochemical cells (PCCs) have recently gained significant attention for applications in energy conversion and storage. Proton conducting ceramics, typically acceptor-doped $Ba(Zr, Ce)O_3$, exhibit a lower activation energy compared to oxygen-ion conductors, enabling high proton conductivity at intermediate temperatures [1,2]. This characteristic allows PCCs to operate at moderate temperatures (400–600°C). In contrast to the high operating temperatures (above 700°C) required for oxygen-ion conductors, the lower operating temperature has the potential to reduce material cost and degradation, thereby enhancing long-term stability and better system integration with respect to heat management.

Electrolytes with reduced thickness can decrease the ohmic resistance in PCCs, further enhancing cell performance at intermediate temperatures, where reaction kinetics are slower. Owing to the advantages of the fuel electrode-supported planar cell design, the thickness of the electrolyte layer can be reduced to just tens of micrometers [3]. Some thin-film fabrication methods allow for the preparation of electrolyte layers as thin as 10 μm or even less [4–7]. It is an obvious advantage that the reduced thickness can significantly shorten the proton transport distance. Additionally, the low grain-boundary proton conductivity of acceptor-doped $Ba(Zr, Ce)O_3$ has long been a major issue, often being several orders of magnitude lower than the bulk conductivity [8,9]. The thin electrolyte layer can have fewer grain boundaries along the proton transport direction, which reduces the impact of slow ionic transport across the grain boundaries. Therefore, the ideal electrolyte layer should be as thin as possible, as long as gas tightness can still be ensured. For example, the ohmic resistance of a 10 μm electrolyte layer differs by an order of magnitude compared to a 1 μm electrolyte layer. Furthermore, if the electrolyte layer thickness is smaller than the grain size, there can be no grain boundary obstacles along the proton transport direction.

Despite the clear theoretical advantages of thin electrolyte layers, reducing the electrolyte layer thickness while ensuring gas tightness is highly challenging from a fabrication perspective. Kim et al. [10] summarized the thickness limitations of various deposition methods for proton-conducting ceramics. They show that apart from vacuum-based physical deposition methods, the thickness limitation of other traditional ceramic thin layer preparation methods is generally above 5 μm. For instance, the electrolyte layers of PCCs prepared by sequential tape casting are typically in the range of 10–30 μm [11–14]. Screen printing can achieve thinner layers, typically in the range of 5–15 μm [15,16]. A few examples demonstrate that traditional layer preparation and sintering can achieve even thinner electrolyte layers [4,10,17], but achieving such reduced thickness imposes stringent requirements on the slurry and the fabrication process. Among the ceramic thin-film deposition methods that are easy to process and suitable for scale-up, the

capability of wet powder spraying (WPS) for preparing thin electrolytes has been largely underestimated. Duan et al. [7] demonstrated the effectiveness of the WPS method by successfully preparing PCCs with ~3.5 μm electrolyte layer, which exhibited excellent electrochemical performance. With the WPS method, the electrolyte thickness can be freely controlled by adjusting the number of spraying passes.

However, excessively thinning the electrolyte layer presents another challenge: The inherent high refractory properties of acceptor-doped Ba(Zr, Ce)O_3 requires sintering temperatures of at least 1400°C [18], where Ba evaporation is another serious issue. Ba evaporation not only negatively affects proton conductivity but also leads to the formation of Y-rich secondary phases, which inhibits the densification and grain growth of the ceramic [19,20]. Specifically, it degrades the surface and near-surface regions of the sample, making this issue particularly detrimental during the sintering of thin electrolyte layers. In this work, we prepared PCCs with electrolyte layers of approximately 3 μm thickness via WPS. To reduce the sintering temperature and mitigate the negative effects of Ba evaporation, we used $SrZr_{0.5}Ce_{0.4}Y_{0.1}O_{3-\delta}$ (SZCY) /NiO as the fuel electrode and substrate material, which has a comparably lower sintering temperature. This not only helps reduce the sintering temperature of the electrolyte, but also allows Sr from the fuel electrode to diffuse into the electrolyte layer, compensating for Ba evaporation. Furthermore, the sintered half-cell was coated with $Ba_{0.5}La_{0.5}CoO_3$ (BLC) as an air electrode and tested in fuel cell mode for I-V curves and power density. Electrochemical impedance spectroscopy was used to study the ohmic and polarization resistance of the full cell. The electrochemical results of our work show that WPS is a promising industrial processing technique to prepare PCCs with thin proton conducting electrolyte layers.

2. Experimental procedure

Commercial powders of SZCY, $BaZr_{0.16}Ce_{0.64}Y_{0.1}Yb_{0.1}O_{3-\delta}$ (BZCYYb) (Kusaka Rare Metal Products Co. Ltd Japan.) and NiO (Vogler) were used in this study. The preparation procedure of the half-cell is illustrated in Figure 1a. The fuel electrode substrate is composed of a functional layer and a support layer. To prepare the tape casting slurry for fuel electrode functional layer, a mixture of 40 wt.% of SZCY and 60 wt.% of NiO was combined with an appropriate amount of organic additive and solvent. The slurry of the fuel electrode support layer used the same recipe but with the addition of 5% of starch relative to the ceramic powder as the pore former. The fuel electrode substrate was prepared by sequential tape casting. The substrate was fabricated by first casting the functional layer, which was dried for 6 hours before the support layer was added. The green tapes were then punched out to round specimens with a diameter of 20 mm. After that, the green tapes were pre-calcined at 900 °C to remove the organics before the electrolyte layer was coated by WPS.

The solution used for WPS was made by mixing the BZCYYb powder with ethanol at a concentration of 2 wt.%. Before spraying, the solution was ultrasonically treated for 30 min. for the WPS

process, the air pressure was set to 160 hPa, the liquid loading rate was 0.033 ml s^{-1} and the spraying nozzle to sample distance was 10 cm. 30 spraying passes were carried out to get the desired thickness. After the coating of BZCYYb electrolyte layer, the half-cell was co-sintered at 1375 °C for 5h. In order to understand the sintering mechanisms, the half-cell was also sintered at 1350 °C for 5h for comparison. Finally, the $Ba_{0.5}La_{0.5}CoO_3$ (BLC) air electrode was coated on the half-cell by screen printing and then sintered at 800 °C for 2h.

The microstructure was characterized by scanning electron microscopy (SEM, EM-30N, Coxem, Ltd. Korea). In order to observe the microstructure of the reduced specimen, the sample was heat-treated in Ar/H_2 at 700 °C for 3h. Samples for scanning transmission electron microscopy (STEM) were prepared using focused ion beam (FIB) to select a specific area (containing grain boundaries). STEM imaging and spectroscopy was done using a probe corrected Hitachi HF5000 microscope (Hitachi High-Technologies, Japan) at 200 keV equipped with an Aztec Energy TEM Advanced EDS System Ultim TLE detector (Oxford Instruments, UK). EDS data analysis and curation were performed using Aztec software (Oxford Instruments, UK).

The current-voltage (IV) curves and impedance spectra of the fabricated cells were evaluated using a potentiostat (Bio-Logic, VMP-250) at temperatures ranging from 500 to 700 °C. The impedance spectra were measured under open circuit voltage (OCV) over a frequency range from 1 MHz to 0.1 Hz, with an AC amplitude of 10 mV. Silver-palladium paste and platinum wires were used as current collectors and leads, respectively. Complete cells were mounted and sealed with Pyrex glass in a Probostat (NorECS, Oslo, Norway). The fuel electrode was supplied with humidified H_2 (3% H_2O) at a flow rate of 100 ml min^{-1}, while the air electrode was exposed to a similar flow rate of ambient air.

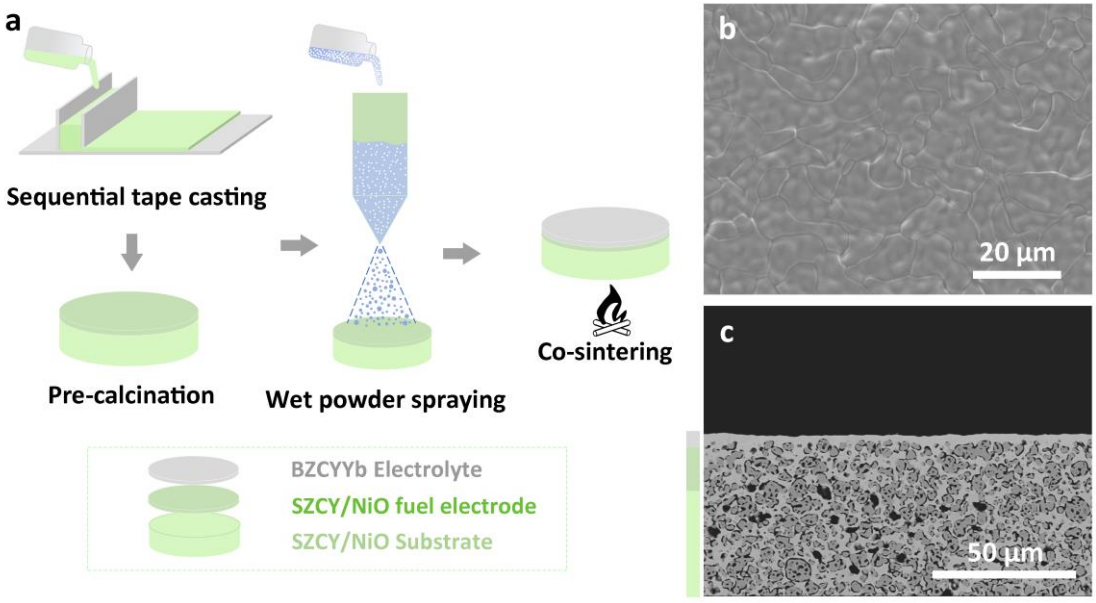

Figure 1. (a) Schematic illustration of the preparation of the half-cell. (b) SEM image of the surface of the BZCYYb electrolyte layer sintered at 1375 °C. (c) SEM image of the polished cross-section of the reduced half-cell that was sintered at 1375 °C.

3. Results and discussion

In the preparation process of PCCs, the co-sintering of the fuel electrode substrate and the electrolyte is the most critical and challenging step. The electrolyte must be sufficiently uniform and dense. However, the issue of poor sinterability and Ba evaporation impose stringent requirements on the structural design, fabrication methods, and sintering process. Figure 1b shows the SEM image of the surface morphology of a sintered BZCYYb electrolyte layer, which was deposited via WPS on a SZCY-based fuel electrode. The BZCYYb layer appears highly dense and shows large grain sizes. The average grain size was determined to be approximately 7.6 μm using the line intersection method on ten SEM images. The sintering temperature of similar compositions in the literature are generally above 1400 °C, typically around 1450 °C. This suggests that the SZCY fuel electrode significantly promotes the sintering and grain growth of the BZCYYb electrolyte. This promotion effect can be attributed to three main factors: (1) the larger shrinkage of the SZCY/NiO substrate during sintering due to its lower sintering temperature [21], which facilitates densification of the BZCYYb layer; (2) Sr diffusion between the fuel electrode and the electrolyte layer during the sintering process, making the final composition of the electrolyte is no longer pure BZCYYb but rather Sr-doped BZCYYb. This modified composition inherently has a lower sintering temperature. Studies by Lee et al. [22] and Sailaja et al. [23] have demonstrated that Sr doping in BZCY facilitates the grain growth; and (3) the compensation of Ba evaporation by Sr diffusion from the substrate, which suppresses the formation of Y-rich secondary phases and promotes larger grain growth.

Since both SZCY and BZCYYb have ABO_3-type perovskite crystal structure, the A-site element interdiffusion between Sr and Ba is inevitable [21]. This interdiffusion plays a crucial role in achieving the densification of the electrolyte layer. Sr and Ba diffusion will be further discussed through STEM characterization. The grain morphology shown in Figure 1b is distinct from that typically observed in sintered BZCYYb electrolyte materials [4,7,20,21,24]. To further validate the role of Sr diffusion in promoting sintering, we conducted additional experiments at a lower sintering temperature of 1350 °C, as shown in Figure 2. The results revealed that the grains sintered at 1350 °C were much smaller, and the electrolyte is not completely dense. Some particles have typical smaller size. The EDS mapping first confirm the Sr is diffused from the fuel electrode to almost all the electrolyte layer. And the smaller particles, further confirmed by EDS point analysis on position 2(the secondary phase), can be identified as Y- , Yb- and Ni-rich secondary phases together with high Sr content and the other elements. The cell sintered at 1350 °C indicating incomplete densification and compositional inhomogeneity. Therefore, the following

inference can be made regarding the sintering of the BZCYYb electrolyte on SZCY. During the sintering process, the evaporation of the A-site element Ba causes the precipitation of the B-site elements Y and Yb. The Sr from the fuel electrode diffuses into the electrolyte layer, compensating for this missing of Ba. However, the diffusion rate of cations is relatively slow at 1350 °C, preventing the electrolyte layer from achieving complete homogenization

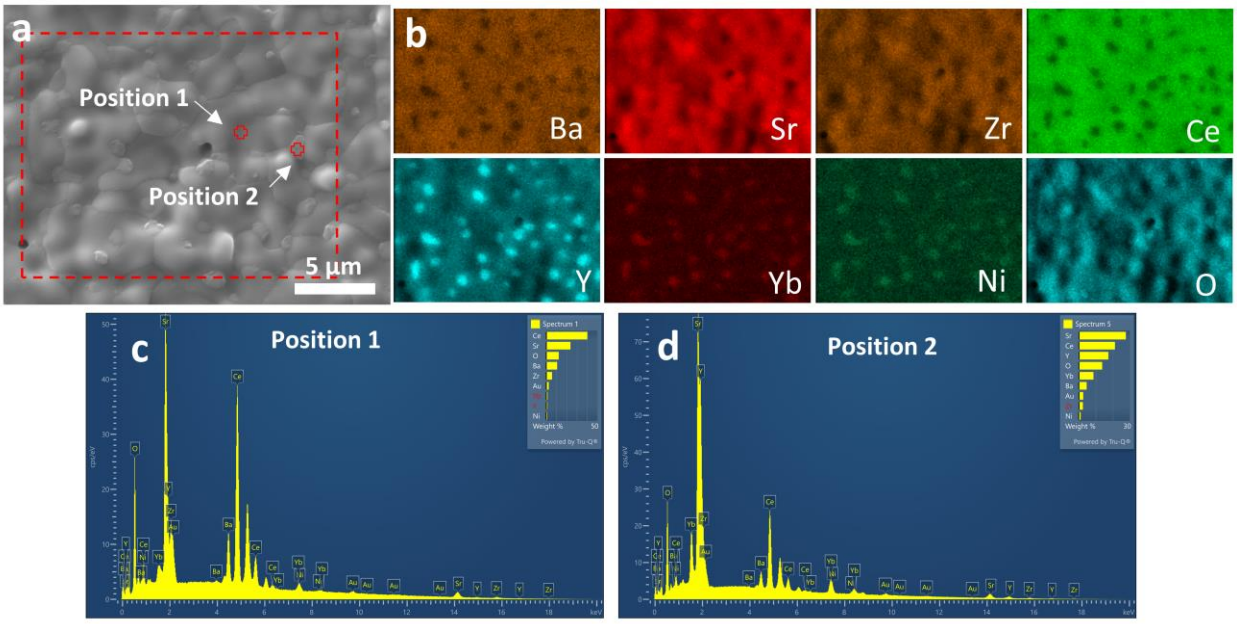

Figure 2. (a) SEM image of the surface of the BZCYYb electrolyte layer sintered at 1350 °C. The EDS mapping area is marked with red dashed rectangular box, and two marked area are for the point EDS analysis. (b) EDS mapping of the selected area. EDS analysis of the point at (c) position 1 and (d) position 2.

Furthermore, no apparent secondary phases were observed in the electrolyte layer sintered at 1375 °C. This confirm that the compensation for Ba evaporation due to Sr diffusion prevents the formation of Y-rich secondary phases in the electrolyte layer that sintered at 1375 °C. According to different reports [19,20,25], it is clear that Ba under-stoichiometry caused by Ba evaporation can result in the formation of Y-rich phases, and typically leads to smaller grain sizes and poor sintering behavior. This phenomenon may be related to a retarding effect of Y-rich phase on grain growth in BZCYYb. With Sr compensation from the substrate, the formation of Y-rich phase is avoided, resulting in large grains after sintering.

Figure 1c shows the polished cross-sectional image of the half-cell after reduction. The entire electrolyte layer is thin and dense, with no evidence of delamination issues post-reduction. A well-connected percolation pathway between the electrolyte layer and the SZCY in the fuel electrode is observed. The fuel electrode functional layer and support layer, which exhibits higher porosity, are distinguishable.

To better investigate the microstructure of the electrolyte layer, STEM characterization was conducted on the half-cell. Figure 3a displays the sampling position during the FIB preparation of the STEM

lamella. Two grain boundaries were deliberately included within the lamella, and the sampling region contained a narrow-grain area. In the STEM bright-field image (Figure 3b), as indicated by the sampling position in Figure 3a, two distinct vertical grain boundaries are clearly visible. There is only one grain present along the proton transport direction. Although the middle grain appears narrow on the surface, no horizontal grain boundaries were observed in the cross-section that could impede proton conduction. The local positive core charge at grain boundaries in proton-conducting ceramics typically acts as a significant barrier to proton transport, leading to much lower grain boundary conductivity compared to the bulk one [26]. However, the structure shown in Figure 3b lacks these grain boundary barriers, which facilitates rapid proton transport through the electrolyte. At the sampling position, the electrolyte layer thickness is approximately 3 μm.

STEM-EDS elemental analysis was performed for the region in Figure 3b. Peak overlapping was prevalent in the EDS spectra due to the large number of elements, such as Yb and Ni. Consequently, the Yb elemental mapping was excluded due to its unreliability. At the selected region, the electrolyte layer was in contact with NiO and SZCY particles from the fuel electrode. It is evident that Ba in the BZCYYb layer had completely interdiffused with Sr in SZCY. Although the partial overlap of Sr and Ce peaks complicated quantification, the uniform signal intensity of Ba and Sr indicates extensive interdiffusion. Moreover, the initial compositions of SZCY and BZCYYb exhibit different Zr/Ce ratios. However, EDS mapping revealed no strong compositional differences in Zr and Ce between these two particles, further confirming substantial elemental exchange between the electrolyte and SZCY in the fuel electrode. This interdiffusion altered the stoichiometry of the electrolyte from its initial composition to a new modified composition with more Sr at A-site. With Sr inclusion, it is expected to exhibit a lower sintering temperature, which further explains the dense microstructure and large grain sizes achieved at 1375 °C. However, Sr-based proton-conducting ceramics typically demonstrate lower proton conductivity compared to their Ba-based counterparts due to a reduced hydration ability [27]. This trade-off represents a compromise strategy for achieving lower sintering temperatures.

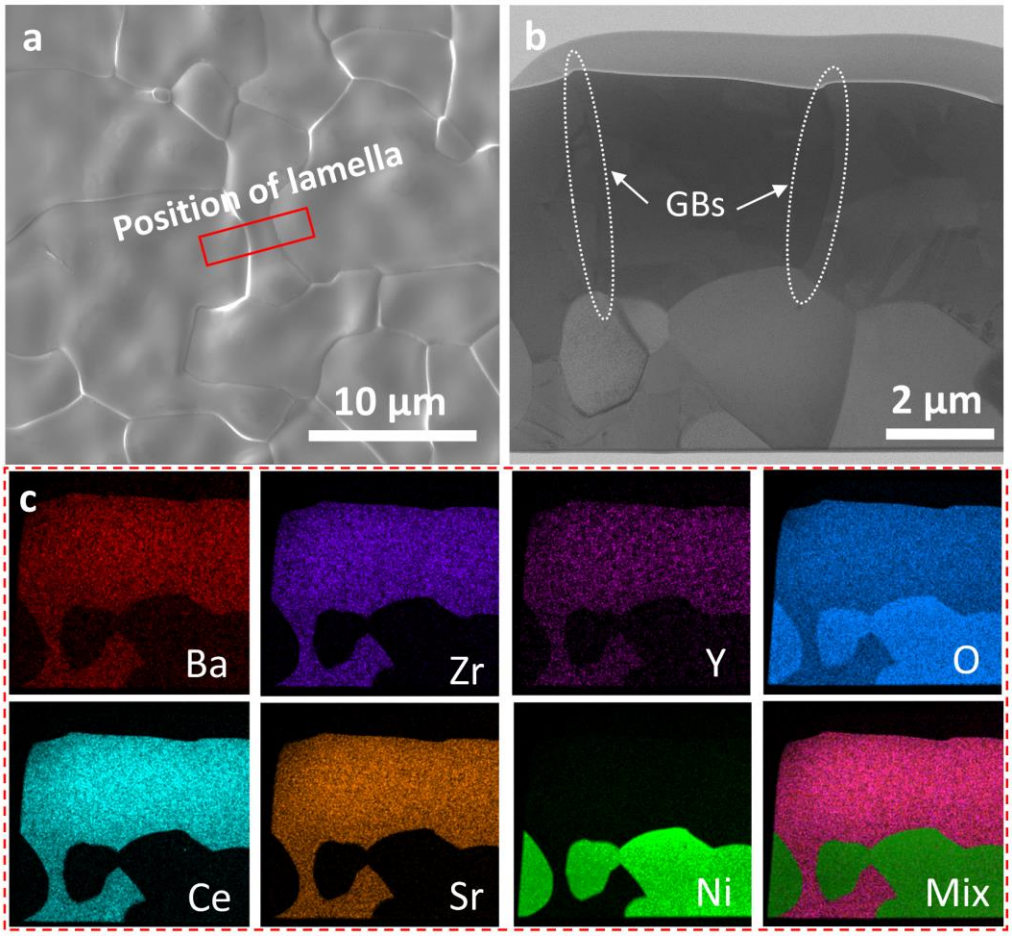

Figure 3. (a) SEM image of the surface of the electrolyte layer sintered at 1375 °C. The area marked by a red rectangle indicates the position where the lamella specimen was prepared by FIB. (b) STEM-bright field image of the electrolyte and fuel electrode (GBs indicate grain boundaries). (c) EDS mapping of the selected area, including Ba, Zr, Y, Ce, Sr, Ni, O.

To perform electrochemical testing of the full cell, BLC was used as the air electrode. Figure 4a shows the cross-sectional fracture surface of the full cell. Figure 4b illustrates the voltage (V) and power density (P) as functions of current density (I) measured at different temperatures (500–700 °C) in fuel cell mode. At 600 °C, the power density achieves 422 mW/cm² at a voltage of 0.7 V. Figure 4c shows the EIS results of the full cell in a Nyquist plot. The ohmic resistance and polarization resistance at different temperatures can be obtained from the plots, which are further plotted as an Arrhenius plot in Figure 4d. At 700 °C, the ohmic resistance of the full cell is 0.19 Ω·cm². The activation energy of the ohmic resistance fitted within the temperature range of 500–700 °C is 0.32 eV, which is similar to the activation energy reported for BZCYYb compositions in the literature [7,22,28]. This relatively low activation energy suggests a favorable ion conduction pathway and indicates that the electrolyte material is well-suited for operation at intermediate temperatures.

At 700 °C, the polarization resistance is lower than the ohmic resistance. However, due to the higher activation energy, the polarization resistance dominates the total resistance when the temperature is below 650 °C. This phenomenon highlights the importance of optimizing both the electrolyte material and the electrode-electrolyte interface to reduce polarization resistance, which becomes a key limiting factor at lower temperatures. It can be observed that the activation energy of the polarization resistance varies in different temperature regions. By segmented fitting, the activation energy is found to be 1.34 eV in the range of 600–700 °C and 0.45 eV in the range of 500–600 °C. The polarization resistance obtained from the single cell includes contributions from both the anode and cathode. Nevertheless, the observed temperature-dependent transition in activation energy is likely related to the behavior of the BLC cathode. This variation, which has also been observed in materials with similar compositions [29,30], is attributed to the different dominant ion transport mechanisms in the BLC air electrode at different temperatures. Oxygen ion transport dominates at higher temperatures, while proton transport becomes dominant at relatively lower temperatures.

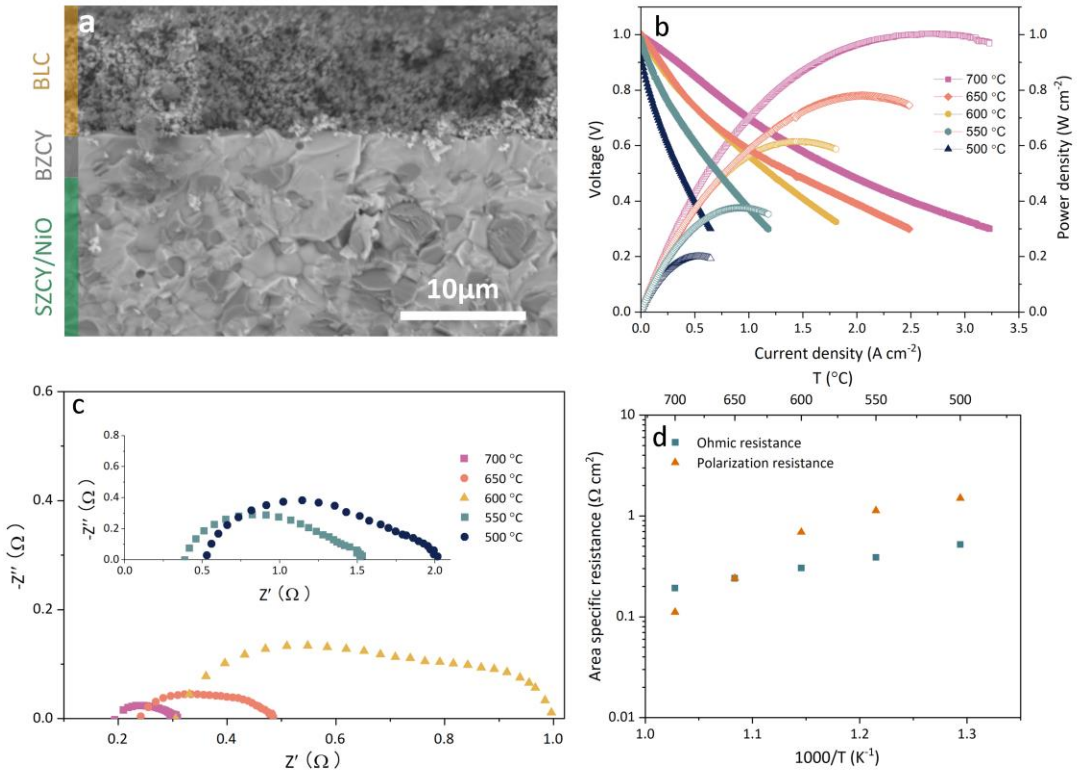

Figure ~~3~~4. (a) SEM image of the fracture surface of the single cell sintered at 1375 °C. (b) The voltage and power density as a function of current density measured at temperature range 500 to 700 °C. (c) Nyquist plots of the full cell measured at temperature range 500 to 700 °C. (d) Arrhenius plots of the ohmic resistance and the polarization resistance.

The reduced ohmic resistance and boosted electrochemical performance brought by the thin electrolyte layer are evident, but some issues have also been exposed. Figure 5 shows the open-circuit voltage (OCV) of the full cell at different temperatures. At 600 °C, the OCV is 1.01 V, slightly lower than the reported values in the literature (1.03, 1.04 V) [7,22]. However, when the temperature decreases to 500 °C, the OCV drops to 0.92 V. Although proton-conducting ceramics are known to exhibit slightly lower OCVs due to electronic leakage caused by electronic conductivity, the electronic conductivity of proton-conducting ceramics should also theoretically decrease as the temperature decreases, leading to a higher OCV. Therefore, the low OCV observed in the tested full cell should not be attributed to electronic leakage. Subsequently, the surface of the sintered electrolyte layer was extensively investigated again, and a few defects were identified that might lead to gas leakage. The inset in Figure 5 shows a specific defect that was discovered. Due to the thinness of the electrolyte layer, even minor defects can result in gas leakage. At high temperatures, rapid reactions may mitigate the impact of these small defects, but as the temperature decreases and gas reaction rates at the interface slow down, the leakage can cause more severe issues. This explains why the OCV decreases as the temperature is lowered.

Nevertheless, these defects are not caused by unreasonable WPS conditions. Before spraying, the substrate undergoes multiple pre-treatments, such as pre-calcination, which can lead to contamination by impurities like dust. Unlike other thin-film deposition methods, WPS involves layer-by-layer deposition of ceramic powder onto the substrate. Any dust or contamination present can be embedded during the spraying process, resulting in defects after sintering. The defect shown in the inset of Figure 5 strongly resembles one caused by a small contaminant covered by subsequent layers. These defects can be avoided through stricter quality control throughout the preparation process or coating in a dust-reduced or -free environment. Especially compared to the rudimentary conditions in a laboratory, a rigorous industrial production process can completely prevent such issues.

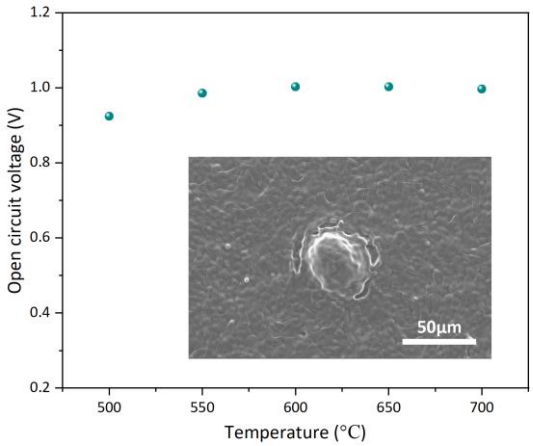

Figure 5. Open circuit voltage of the full cell at different measurement temperatures. Insert SEM image present one example of defect on the electrolyte surface that may lead to gas leakage.

Conclusion

This study highlights the feasibility of fabricating thin proton-conducting electrolyte layers using the wet powder spraying method for high-temperature PCCs. The co-sintering of a 3 μm BZCYYb electrolyte layer on an SZCY/NiO substrate at 1375 °C resulted in a dense microstructure with large grain sizes, benefiting from Sr diffusion, that mitigates Ba evaporation. Electrochemical testing demonstrated a power density of 422 mW/cm² at 0.7 V and 600 °C, with low ohmic and polarization resistance. STEM analysis revealed that elemental interdiffusion between the electrolyte and substrate enhanced sinterability and influenced the composition and microstructure of the electrolyte. Despite the promising results, minor defects in the electrolyte layer led to reduced OCVs, particularly at lower temperatures. These defects stemmed from contamination during substrate preparation, rather than limitations of the WPS method. This work offers valuable insights into addressing the challenges of thin electrolyte fabrication and advancing PCC technology.

Acknowledgement

This study was supported by the Chinese Scholarship Council (CSC) and the Helmholtz Research Program ‘‘Materials and Technologies for the Energy Transition’’ (MTET) funded by the German Ministry of Education and Research (BMBF).

Data availability

Data will be made available on request.

References

[1] K. Singh, R. Kannan, V. Thangadurai, Perspective of perovskite-type oxides for proton conducting solid oxide fuel cells, Solid State Ionics 339 (2019) 114951. https://doi.org/10.1016/j.ssi.2019.04.014.

[2] S. Guo, L. Jiang, Y. Li, P. Zhong, S. A. Ismail, T. Norby, D. Han, From Electrolyte and Electrode Materials to Large - Area Protonic Ceramic Fuel Cells: A Review. Advanced Functional Materials 32(2024) 34. https://doi.org/10.1002/adfm.202304729.

[3] J. Zhang, S. Ricote, P.V. Hendriksen, Y. Chen, Advanced Materials for Thin-Film Solid Oxide Fuel Cells: Recent Progress and Challenges in Boosting the Device Performance at Low Temperatures, Advanced Functional Materials 32 (2022) 2111205. https://doi.org/10.1002/adfm.202111205.

[4] H. An, H.-W. Lee, B.-K. Kim, J.-W. Son, K.J. Yoon, H. Kim, D. Shin, H.-I. Ji, J.-H. Lee, A 5 × 5 cm^2 protonic ceramic fuel cell with a power density of 1.3 W cm^{-2} at 600 °C, Nat Energy 3 (2018) 870–875. https://doi.org/10.1038/s41560-018-0230-0.

[5] J. Zhang, C. Lenser, N. Russner, A. Weber, N.H. Menzler, O. Guillon, Boosting intermediate temperature performance of solid oxide fuel cells via a tri-layer ceria–zirconia–ceria electrolyte, J Am Ceram Soc. 106 (2023) 93–99. https://doi.org/10.1111/jace.18482.

[6] F. Han, R. Mücke, T. Van Gestel, A. Leonide, N.H. Menzler, H.P. Buchkremer, D. Stöver, Novel high-performance solid oxide fuel cells with bulk ionic conductance dominated thin-film electrolytes, Journal of Power Sources 218 (2012) 157–162. https://doi.org/10.1016/j.jpowsour.2012.06.087.

[7] F. Liu, H. Deng, D. Diercks, P. Kumar, M.H.A. Jabbar, C. Gumeci, Y. Furuya, N. Dale, T. Oku, M. Usuda, P. Kazempoor, L. Fang, D. Chen, B. Liu, C. Duan, Lowering the operating temperature of protonic ceramic electrochemical cells to <450 °C, Nat Energy (2023). https://doi.org/10.1038/s41560-023-01350-4.

[8] G. Qin, J. Bao, J. Gao, F. Ruan, S. An, Z. Wang, L. Li, Enhanced grain boundary conductivity of Gd and Sc co-doping $BaZrO_3$ proton conductor for proton ceramic fuel cell, Chemical Engineering Journal 466 (2023) 143114. https://doi.org/10.1016/j.cej.2023.143114.

[9] F. Iguchi, T. Tsurui, N. Sata, Y. Nagao, H. Yugami, The relationship between chemical composition distributions and specific grain boundary conductivity in Y-doped $BaZrO_3$ proton conductors, Solid State Ionics 180 (2009) 563–568. https://doi.org/10.1016/j.ssi.2008.12.006.

[10] Y.S. Kim, W. Chang, H.J. Jeong, K.H. Kim, H.S. Park, J.H. Shim, High performance of protonic ceramic fuel cells with 1-μm-thick electrolytes fabricated by inkjet printing, Additive Manufacturing 71 (2023) 103590. https://doi.org/10.1016/j.addma.2023.103590.

[11] K. Leonard, M.E. Ivanova, A. Weber, W. Deibert, W.A. Meulenberg, T. Ishihara, H. Matsumoto, Anode supported planar 5 × 5 cm^2 $SrZr_{0.5}Ce_{0.4}Y_{0.1}O_{2.95}$ based solid oxide protonic fuel cells via sequential tape-casting, Solid State Ionics 379 (2022) 115918. https://doi.org/10.1016/j.ssi.2022.115918.

[12] Z. Huang, Y. Yang, H. Lv, C. Shi, T. Li, Y. Ling, T. Chen, S. Wang, Large-area anode-supported protonic ceramic fuel cells combining with multilayer-tape casting and hot-pressing lamination technology, Journal of the European Ceramic Society 43 (2023) 428–437. https://doi.org/10.1016/j.jeurceramsoc.2022.09.057.

[13] H. Zhang, Y. Zhou, K. Pei, Y. Pan, K. Xu, Y. Ding, B. Zhao, K. Sasaki, Y. Choi, Y. Chen, M. Liu, An efficient and durable anode for ammonia protonic ceramic fuel cells, Energy Environ. Sci. 15 (2022) 287–295. https://doi.org/10.1039/D1EE02158C.

[14] Y. Ma, J. Huang, B. He, Scalable fabrication process for new structure $BaZr_{0.8}Y_{0.2}O_{3-\delta}$-based protonic ceramic fuel cells, Ceramics International 47 (2021) 14680–14688. https://doi.org/10.1016/j.ceramint.2021.01.264.

[15] S.M. Choi, J.-H. Lee, H.I. Ji, K.J. Yoon, J.-W. Son, B.-K. Kim, H.J. Je, H.-W. Lee, J.-H. Lee, Fabrication and characterization of $Ba(Zr_{0.84}Y_{0.15}Cu_{0.01})O_3$ electrolyte-based protonic ceramic fuel cells, Ceramics International 39 (2013) 9605–9611. https://doi.org/10.1016/j.ceramint.2013.05.081.

[16] S. Hossain, A.M. Abdalla, J.H. Zaini, C.D. Savaniu, J.T.S. Irvine, A.K. Azad, Highly dense and novel proton conducting materials for SOFC electrolyte, International Journal of Hydrogen Energy 42 (2017) 27308–27322. https://doi.org/10.1016/j.ijhydene.2017.09.067.

[17] S.M. Choi, H. An, K.J. Yoon, B.-K. Kim, H.-W. Lee, J.-W. Son, H. Kim, D. Shin, H.-I. Ji, J.-H. Lee, Electrochemical analysis of high-performance protonic ceramic fuel cells based on a columnar-structured thin electrolyte, Applied Energy 233–234 (2019) 29–36. https://doi.org/10.1016/j.apenergy.2018.10.043.

[18] F.J.A. Loureiro, N. Nasani, G.S. Reddy, N.R. Munirathnam, D.P. Fagg, A review on sintering technology of proton conducting $BaCeO_3$-$BaZrO_3$ perovskite oxide materials for Protonic Ceramic Fuel Cells, Journal of Power Sources 438 (2019) 226991. https://doi.org/10.1016/j.jpowsour.2019.226991.

[19] Y. Zeng, M. Kindelmann, K. Leonard, L.-A. Schäfer, K. Yao, J. Malzbender, M. Müller, O. Guillon, M.E. Ivanova, N.H. Menzler, Characterization of high Zr/Ce ratio $Ba(Zr,Ce,Y)O_{3-\delta}$ proton conductors: investigating the impact of Y on the properties of materials, Phys. Chem. Chem. Phys. 27 (2025) 885–896. https://doi.org/10.1039/D4CP04384G.

[20] M. Choi, J. Paik, D. Kim, D. Woo, J. Lee, S.J. Kim, J. Lee, W. Lee, Exceptionally high performance of protonic ceramic fuel cells with stoichiometric electrolytes, Energy Environ. Sci. 14 (2021) 6476–6483. https://doi.org/10.1039/D1EE01497H.

[21] K. Leonard, Y. Okuyama, Y. Takamura, Y.-S. Lee, K. Miyazaki, M.E. Ivanova, W.A. Meulenberg, H. Matsumoto, Efficient intermediate-temperature steam electrolysis with Y : $SrZrO_3$ –$SrCeO_3$ and Y : $BaZrO_3$ – $BaCeO_3$ proton conducting perovskites, J. Mater. Chem. A 6 (2018) 19113–19124. https://doi.org/10.1039/C8TA04019B.

[22] K.-R. Lee, C.-J. Tseng, J.-K. Chang, I.-M. Hung, J.-C. Lin, S.-W. Lee, Strontium doping effect on phase homogeneity and conductivity of $Ba_{1-x}Sr_xCe_{0.6}Zr_{0.2}Y_{0.2}O_{3-\delta}$ proton-conducting oxides, International Journal of Hydrogen Energy 38 (2013) 11097–11103. https://doi.org/10.1016/j.ijhydene.2013.01.043.

[23] J. Madhuri Sailaja, N. Murali, K. Vijay Babu, V. Veeraiah, Effect of Strontium the phase structure of $Ba_{1-x}Sr_x$ $Ce_{0.65}Zr_{0.2}Y_{0.15}O_{3-\delta}$ ($0 \le x \le 0.25$) proton conductor by citrate–EDTA complexing sol–gel method, Journal of Asian Ceramic Societies 5 (2017) 18–30. https://doi.org/10.1016/j.jascer.2016.12.004.

[24] W. Bian, W. Wu, B. Wang, W. Tang, M. Zhou, C. Jin, H. Ding, W. Fan, Y. Dong, J. Li, D. Ding, Revitalizing interface in protonic ceramic cells by acid etch, Nature 604 (2022) 479–485. https://doi.org/10.1038/s41586-022-04457-y.

[25] J.N. Ebert, D. Jennings, W.S. Scheld, D. Sebold, W. Rheinheimer, Influence of Ba non-stoichiometry on the processing properties of Y- and Sc-doped $BaZrO_3$, Journal of the European Ceramic Society 44 (2024) 6995–7005. https://doi.org/10.1016/j.jeurceramsoc.2024.04.070.

[26] M. Kindelmann, I. Povstugar, S. Kuffer, D. Jennings, J.N. Ebert, M.L. Weber, M.P. Zahler, S. Escolastico, L. Almar, J.M. Serra, P. Kaghazchi, M. Bram, W. Rheinheimer, J. Mayer, O. Guillon, Controlling Grain Boundary Segregation to Tune the Conductivity of Ceramic Proton Conductors, Advanced Energy Materials (2024) 2404410. https://doi.org/10.1002/aenm.202404410.

[27] K. Leonard, Y.-S. Lee, Y. Okuyama, K. Miyazaki, H. Matsumoto, Influence of dopant levels on the hydration properties of SZCY and BZCY proton conducting ceramics for hydrogen production, International Journal of Hydrogen Energy 42 (2017) 3926–3937. https://doi.org/10.1016/j.ijhydene.2016.10.120.

[28] M. Zhou, Z. Liu, M. Chen, Z. Zhu, D. Cao, J. Liu, Electrochemical performance and chemical stability of proton-conducting $BaZr_{0.8-x}Ce_xY_{0.2}O_{3-\delta}$ electrolytes, J Am Ceram Soc. (2022) jace.18500. https://doi.org/10.1111/jace.18500.

[29] R. Strandbakke, E. Vøllestad, S.A. Robinson, M.-L. Fontaine, T. Norby, $Ba_{0.5}Gd_{0.8}La_{0.7}Co_2O_{6-\delta}$ Infiltrated in Porous $BaZr_{0.7}Ce_{0.2}Y_{0.1}O_3$ Backbones as Electrode Material for Proton Ceramic Electrolytes, J. Electrochem. Soc. 164 (2017) F196–F202. https://doi.org/10.1149/2.0141704jes.

[30] R. Strandbakke, V.A. Cherepanov, A.Yu. Zuev, D.S. Tsvetkov, C. Argirusis, G. Sourkouni, S. Prünte, T. Norby, Gd- and Pr-based double perovskite cobaltites as oxygen electrodes for proton ceramic fuel cells and electrolyser cells, Solid State Ionics 278 (2015) 120–132. https://doi.org/10.1016/j.ssi.2015.05.014.